



Shigella promotes major alteration of gut epithelial physiology and tissue invasion by shutting off host intracellular transport

Mariana Ferrari, Valérie Malardé, Laura Salavessa, Giulia Nigro, Stéphane Descorps-Declère, John Rohde, Pamela Schnupf, Vanessa Masson, Guillaume Arras, Damarys Loew, et al.

► To cite this version:

Mariana Ferrari, Valérie Malardé, Laura Salavessa, Giulia Nigro, Stéphane Descorps-Declère, et al.. Shigella promotes major alteration of gut epithelial physiology and tissue invasion by shutting off host intracellular transport. Proceedings of the National Academy of Sciences of the United States of America, 2019, 10.1073/pnas.1902922116 . pasteur-02167942

HAL Id: pasteur-02167942

<https://pasteur.hal.science/pasteur-02167942>

Submitted on 3 Jun 2020

HAL is a multi-disciplinary open access archive for the deposit and dissemination of scientific research documents, whether they are published or not. The documents may come from teaching and research institutions in France or abroad, or from public or private research centers.

L'archive ouverte pluridisciplinaire **HAL**, est destinée au dépôt et à la diffusion de documents scientifiques de niveau recherche, publiés ou non, émanant des établissements d'enseignement et de recherche français ou étrangers, des laboratoires publics ou privés.

Shigella promotes major alteration of gut epithelial physiology and tissue invasion by shutting off host intracellular transport

Mariana L. Ferrari^{1,2}, Valérie Malardé^{1,2}, Alexandre Grassart^{1,2}, Laura Salavessa^{1,2,3}, Giulia Nigro^{1,2}, Stéphane Decorps-Declere⁴, John R. Rohde⁵, Pamela Schnupf⁶, Vanessa Masson⁷, Guillaume Arras⁷, Damarys Loew⁷, Philippe J. Sansonetti^{1,2,8*}, Nathalie Sauvonnnet^{1,2*}

¹ Unité de Pathogénie Microbienne Moléculaire, Institut Pasteur, 28 rue du Dr Roux, 75015, Paris, France ² U1202, INSERM, Paris, France ³ Université Paris Sud, Paris-Saclay University, Orsay, France ⁴ Institut Pasteur – Hub Bioinformatique et Biostatistique – C3BI, USR 3756 IP CNRS – 28 rue du Dr Roux, 75015, Paris, France ⁵ Department of Microbiology and Immunology, Dalhousie University, Halifax, NS, Canada ⁶ Institut Necker Enfants Malades, INSERM-CNRS, Laboratory of Host-Microbiota Interaction, 156 rue de Vaugirard, 75015 Paris, France ⁷ Institut Curie, PSL Research University, Centre de Recherche, Laboratoire de Spectrométrie de Masse Protéomique, 26 rue d'Ulm, Paris 75248 Cedex 05, France ⁸ Chaire de Microbiologie et Maladies Infectieuses, Collège de France, Paris, France

Submitted to Proceedings of the National Academy of Sciences of the United States of America

Intracellular trafficking pathways in eukaryotic cells are essential to maintain organelle identity and structure, and to regulate cell communication with its environment. *Shigella flexneri* invades and subverts the human colonic epithelium by the injection of virulence factors through a type 3 secretion system (T3SS). In this work we report the multiple effects of two *S. flexneri* effectors, IpaJ and VirA, which target small GTPases of the Arf and Rab families, consequently inhibiting several intracellular trafficking pathways. IpaJ and VirA induce large-scale impairment of host protein secretion and block the recycling of surface receptors. Moreover, these two effectors decrease clathrin-dependent and -independent endocytosis. Therefore, *S. flexneri* infection induces a global blockage of host cell intracellular transport, affecting the exchange between cells and their external environment. The combined action of these effectors disorganizes the epithelial cell polarity, disturbs epithelial barrier integrity, promotes multiple invasion events and enhances the pathogen capacity to penetrate into the colonic tissue *in vivo*.

bacteria | pathogen | secretion | endocytosis | polarity

Introduction

Eukaryotic cells contain a complex array of intracellular membrane-bound compartments, which mediate cell communication with their environment by the bi-directional transport of proteins and lipids between the intracellular and extracellular spaces. This occurs via two main mechanisms: the secretory and the endocytic trafficking pathways. The efficient intracellular transport of molecules is regulated by GTPases of the Arf, Rab, Rho and dynamin families and is critical to maintain organelle identity and structure. Additionally, the coordination of intracellular trafficking with other pathways regulates vital processes including cell polarity, immunity, signaling and development as well as tissue and organ functions (1–3).

Shigella spp are Gram-negative intracellular bacteria causing bacillary dysentery or shigellosis (4). *Shigella* invades the colonic epithelium by using a type 3 secretion system (T3SS) that enables the injection of more than 20 virulence factors, the so-called effectors, into the cell (5, 6). These effectors then target multiple cellular functions to promote non-phagocytic uptake, followed by intracellular bacterial replication, cell-to-cell spreading, and subsequently leading to destruction of the colonic epithelium (7, 8). While the enzymatic functions for most effectors has been described and analyzed in cell culture, the mechanisms by which they cooperate with one another to promote infection remains largely unknown. *S. flexneri* induces Golgi apparatus fragmentation and reorganization of the endocytic compartment, leading to a block in secretion and receptor recycling (9). Among the

arsenal of injected effectors, two have been specifically implicated in targeting host cell small GTPases essential for Golgi-mediated secretory transport, namely: IpaJ and VirA. IpaJ is a cysteine protease catalyzing the cleavage of myristoylated glycine residues primarily from ADP-ribosylation factor (Arf) and Arf-like (Arl) proteins (10, 11). As a consequence, it was shown that IpaJ inhibits STING-mediated activation of the interferon (IFN) pathway by blocking STING translocation from the endoplasmic reticulum (ER) to ER-Golgi intermediate compartment (ERGIC) (12). Conversely, VirA was reported to impair host cell secretory transport, in addition to inhibiting autophagy (13, 14), by acting as a Rab-GTP activating protein (GAP) with preferential targeting of Rab1, as shown *in vitro* (13). Although the catalytic activities of these two effectors have been well described, it remains to be elucidated if both act in synergy or independently, and which changes they induce in the intestinal tissue during *S. flexneri* infection.

In eukaryotes, Arf and Rab protein families work together to regulate intracellular trafficking pathways. However, the exact mechanisms of coordination of action are not yet fully understood. Given that these small GTPases are targeted by both IpaJ

Significance

Shigella flexneri is an enteroinvasive prokaryote that induces human bacillary dysentery. The delivery of around 30 bacterial effectors inside colonic epithelial cells allows the pathogen to invade, replicate and move into adjacent cells, hence subverting cellular and immune functions of its host. Intracellular trafficking pathways in eukaryotic cells are essential to regulate cell communication with their environment. Our work shows that two effectors of *Shigella flexneri* block three main trafficking pathways of its host cell: secretion, recycling and endocytosis, thereby freezing the exchange through the plasma membrane. As a consequence, *Shigella flexneri* disorganizes the epithelial cell polarity, disturbs epithelial barrier integrity, and enhances the pathogen capacity to penetrate into the colonic tissue *in vivo*.

Reserved for Publication Footnotes

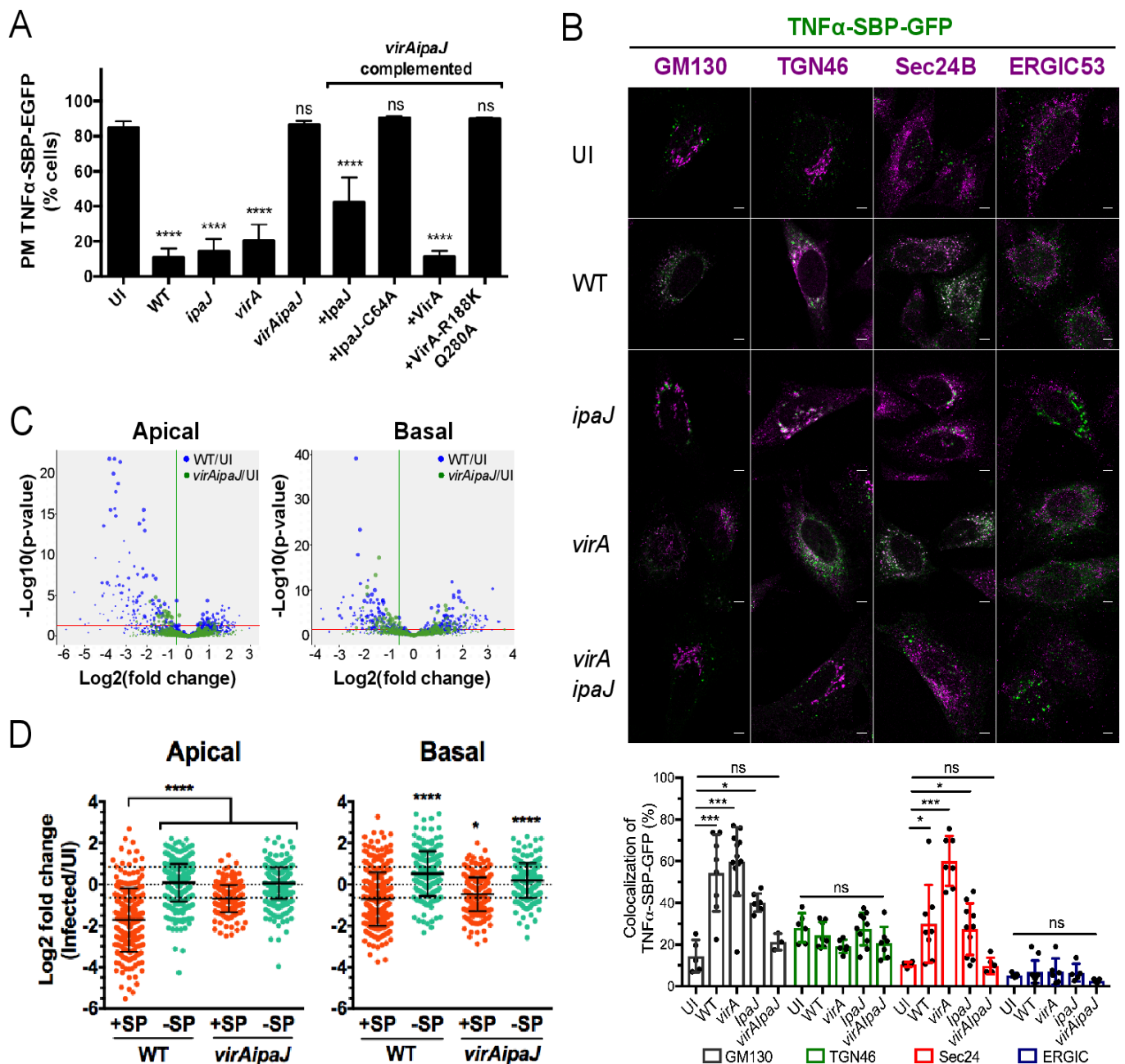


Fig. 1. *S. flexneri* effectors IpaJ and VirA have a global effect on conventional secretion. (A) IpaJ and VirA effectors block the anterograde transport of the cytokine TNF α . HeLa cells stably expressing the RUSH cargo TNF α -SBP-GFP and the molecular hook Streptavidin-KDEL were uninfected (UI) or infected for 1 hour with WT-dsRed or the dsRed-expressing mutants *ipaJ*, *virA*, *virAipaJ*, or with *virAipaJ* complemented with *plpA*-myc, *plpA*-C64-myc, *pVirA*-myc, or *pVirA-R188K/Q280A*-myc. Cells were then incubated with biotin for 1 hour, fixed and surface-stained for TNF α -SBP-GFP with anti-GFP DyLight 680 conjugated antibody. The arrival of TNF α -SBP-GFP to the plasma membrane (PM) was monitored by flow cytometry. Mean SD. $n = 3$. **** $p < 0.0001$, ns: non-significant (one-way ANOVA, Dunnett's *post-hoc* test, compared to UI). (B) TNF α -SBP-GFP is retained in different subcellular compartments upon *S. flexneri* infection. HeLa cells stably expressing the RUSH cargo TNF α -SBP-GFP and the molecular hook Streptavidin-KDEL were uninfected (UI) or infected for 1 hour and incubated with biotin for 1 additional hour. Cells were fixed, permeabilized and stained with various subcellular markers: anti-GM130 (*cis*-Golgi), anti-ERGIC53 (ERGIC), anti-Sec24B (ERES), anti-TGN46 (*trans*-Golgi network). Scale bar: 5 μ m. Levels of colocalization between TNF α -SBP-GFP and the different sub-cellular markers were quantified by SODA plugin in ICY software. Mean SD, $5 < n < 12$ cells. * $p < 0.05$; *** $p < 0.001$ (one-way ANOVA, Dunnett's *post-hoc* test). (C-D) *S. flexneri* blocks globally the host conventional secretion. Caco-2/TC7 cells were labeled with SILAC amino acids, grown in transwell filters and infected with WT *S. flexneri* or the mutant *virAipaJ*. After 4.5 hours, the apical and basal media were collected and analyzed by mass spectrometry to determine the relative abundance of secreted proteins in the infected, in comparison with UI samples. (C) Volcano plots displaying log₂ fold-changes of secreted proteins from WT or *virAipaJ* infected cells in comparison with UI conditions in apical and basal media. (D) Dot plots represent log₂ of infected/UI ratio for proteins with (red) and without (green) signal peptide (SP). Mean SD. 217 $>$ 394 proteins for Apical secretome; 194 $>$ 281 proteins for Basal secretome. * $p < 0.05$, **** $p < 0.0001$ (one-way ANOVA, Dunnett's *post-hoc* test, each condition compared to Apical or Basal secreted proteins containing signal peptide (+SP)).

and VirA, it raises the question if these effectors further affect

other trafficking pathways in addition to the known secretory transport.

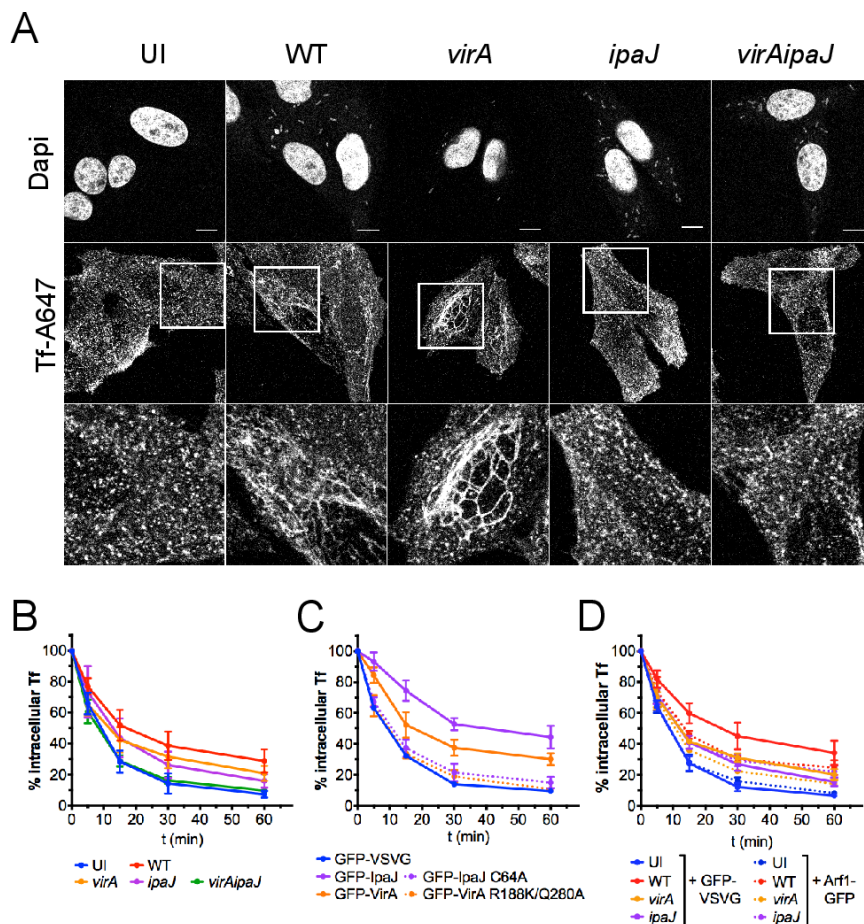


Fig. 2. Both *S. flexneri* IpaJ and VirA affect TfR recycling. (A) IpaJ induces endosomal tubulation. Hep2 cells loaded with Tf-AF647 were uninfected (UI) or infected for 1 hour with WT, *virA*, *ipaJ* or *virAipaJ* strains, fixed and stained with Dapi (nuclei and bacteria). Scale bar: 10 μ m. (B-D) Tf recycling kinetics monitored by FC. Hep2 cells non-transfected or transfected with the indicated plasmids were loaded with Tf-AF647 and were left UI or infected for 1 hour with the indicated *S. flexneri* strains. Cells were then chased with unlabeled holo-Tf, and the loss of intracellular Tf-AF647 fluorescence was monitored over time. (B) IpaJ and VirA block Tf recycling. Cells were UI or infected with WT, *virA*, *ipaJ* or *virAipaJ* strains followed by Tf recycling kinetic. (C) Tf recycling is inhibited by IpaJ and VirA catalytic activities. Cells were transfected with GFP-VSVG (control), GFP-VirA, GFP-IpaJ or their mutated versions GFP-VirA-R188K/Q280A and GFP-IpaJ-C64A. Tf recycling kinetic was performed 24 hours post-transfection. (D) Arf1-GFP overexpression partially recovers Tf recycling. Cells were transfected either with GFP-VSVG (control) or Arf1-GFP, loaded with Tf-AF647, UI or infected with WT, *virA* or *ipaJ* strains followed by Tf recycling. Means SD from at least 3 independent experiments are shown (statistical tests in Fig. S2D-F).

Here, we demonstrate that these two effectors independently block global host cell secretion and concurrently operate to impair receptor recycling. Moreover, we report that IpaJ and VirA decrease receptor-mediated endocytosis. Our results illustrate how *S. flexneri* “freezes” the invaded host cell by globally interfering on multiple intracellular transport systems, thereby affecting the exchange of molecules between cells and their environment and consequently cell and tissue functions.

Results

S. flexneri effectors IpaJ and VirA globally impair conventional secretion

Both IpaJ and VirA *S. flexneri* effectors have been shown to affect Golgi-mediated transport in host cells (10, 13), raising the question as to whether these effectors operate in synergy or independently. To address this, we first quantified the secretion level of the cytokine TNF α upon infection with wild type (WT) *S. flexneri*, or the mutant strains *ipaJ*, *virA*, or *virAipaJ*. We used the RUSH system (15) to follow the synchronized trafficking of the reporter TNF α -SBP-GFP from the endoplasmic reticulum to the plasma membrane of epithelial cells (Fig. 1A). Infection with WT *S. flexneri* blocked 75% of the anterograde trafficking of TNF α -SBP-GFP when compared to uninfected cells (UI), in line with previous reports on other cargoes (9, 13). Similar results were obtained when cells were infected with either *ipaJ* or *virA* *S. flexneri* single mutants. However, in cells infected by the *virAipaJ* double mutant, TNF α -SBP-GFP transport levels were similar to the uninfected condition (Fig. 1A). This differential effect of trafficking during infection by WT, *ipaJ*, *virA* and *virAipaJ* was not due to impairment in bacterial invasion by the mutant strains (Fig.

S1A). Complementation of the double mutant with either pVirA-myc or pIpaJ-myc was sufficient to restore, at least partially, the secretion inhibitory phenotype obtained with WT bacteria. As expected, complementation with the mutated versions of these effectors in their catalytic sites, pVirA-R188K/Q280A-myc or pIpaJ-C64A-myc (10, 13), did not affect the normal trafficking of TNF α -SBP-GFP (Fig. 1A). Altogether, these results show that each effector, IpaJ and VirA, is sufficient to block anterograde transport of the cargo via their catalytic activities and hence acts largely independently.

To determine in which subcellular compartment TNF α -SBP-GFP was retained upon *S. flexneri* infection, we utilized immunostaining of various subcellular compartments after 1 hour of synchronized trafficking and quantified the percentage of colocalization using a statistical object-based method (Fig. 1B). In uninfected and *virAipaJ* infected cells, TNF α -SBP-GFP was mostly at plasma membrane (Fig. 1A), but the minor intracellular pool was mostly colocalized with *trans*-Golgi network (TGN) labeled with TGN46 (21-28%) and with *cis*-Golgi remnants (GM130-positive compartment, 14-20%) (Fig. 1B). By contrast, in WT-infected cells TNF α -SBP-GFP was mostly intracellular (Fig. 1A) and colocalized with GM130 (54%), Sec24B (29%), a marker of ER exit sites (ERES), and with TGN46 (24%). This reveals that *S. flexneri* WT infection blocked the Golgi-mediated transport at different stages, mainly at ERES and at *cis*-Golgi. Interestingly, infection with *virA* or *ipaJ* mutants resulted in a phenotype similar to the WT strain except that in absence of IpaJ, TNF α -SBP-GFP was strongly colocalized with Sec24 (60%, Fig. 1B). These data suggest that the retention in the Sec24B-positive compartment was due to the action of IpaJ. We could not observe colocalization

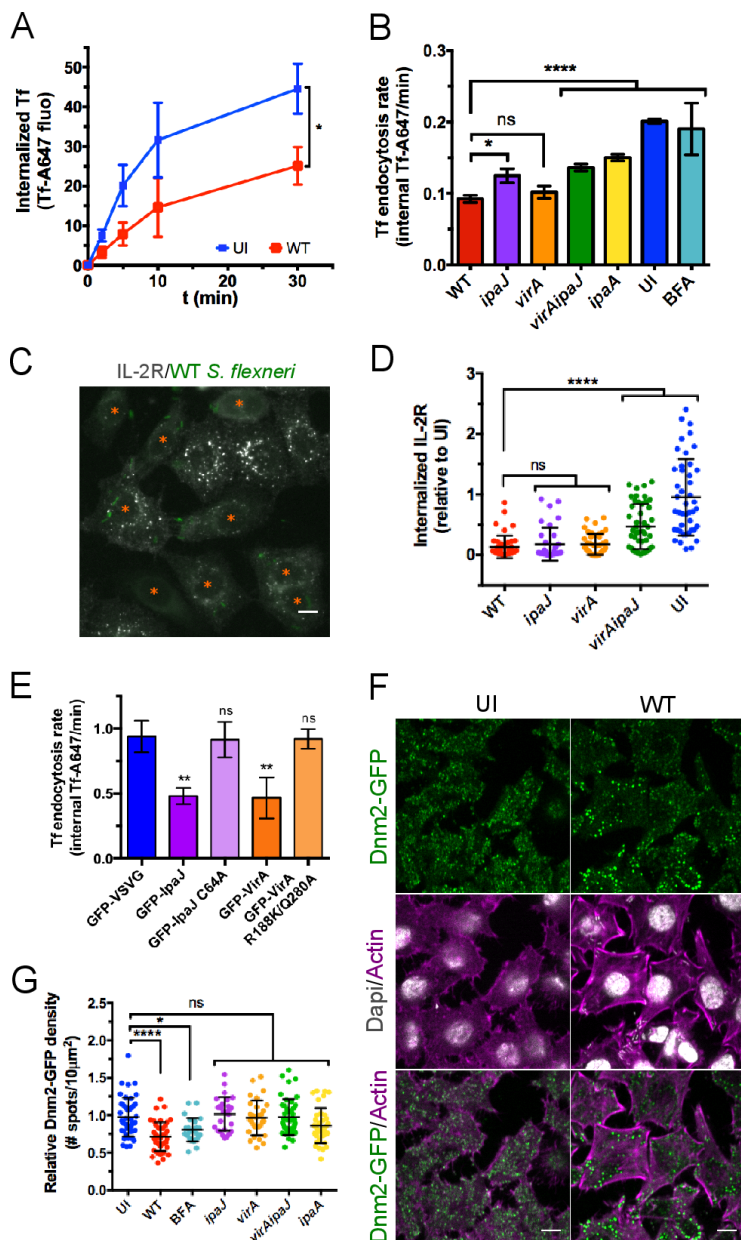


Fig. 3. *S. flexneri* affects clathrin-dependent and independent endocytosis. (A) Tf uptake is decreased upon WT-infection. Hep2 cells were left uninfected (UI) or infected with the WT strain for 30 min and then incubated for different time-points with Tf-AF647 at 37 °C. After an acidic wash, the total internal Tf-AF647 fluorescence was quantified by FC. Mean SD, n = 4. *p<0.05 (unpaired two-tailed Welch's t-test performed on AUC). **(B)** Different *S. flexneri* effectors decrease the Tf endocytosis rate. Hep2 cells were left UI or infected with GFP-expressing WT or mutant strains for 90 min, prior to monitor by FC the Tf-AF647 uptake over time. Mean SD, n = 3. **(C-D)** IL-2R endocytosis is decreased upon WT *S. flexneri* infection. **(C)** UI or WT-infected Hep2 cells were incubated with an anti-IL-2Rβ-Cy3 antibody for 15 min at 37°C, fixed and subjected to fluorescent microscopy. Scale bar: 10 μm. **(D)** Quantification of IL-2R endocytosis. Cells either UI or infected by WT, *ipaJ*, *virA* and *virAipaJ* *S. flexneri* strains for 90 min were incubated with an anti-IL-2Rβ-Cy3 antibody for 30 min at 37°C, fixed, subjected to confocal fluorescence microscopy and analyzed by quantifying the fluorescence intensity of IL-2R-positive vesicles per cell. Mean SD, 35<n<48 cells. **(E)** Tf endocytosis kinetic was performed 24 hours post-transfection. Mean SD, n = 3. **(F-G)** *S. flexneri* decrease Dnm2-GFP density at plasma membrane. Hep2β Dnm2-GFP cells were UI, treated with BFA for 30 min or infected with WT or mutant strains for 90 min. Cells were fixed and labeled with rabbit anti-LPS followed by anti-rabbit-A405 and Phalloidin-A647 prior to confocal **(F)** or TIRF **(G)** imaging. Scale bar: 10 μm. **(G)** Quantification of Dnm2-GFP density (number of Dnm2-GFP spots/area) at plasma membrane from TIRF microscopy images. Mean SD, 27<n<45 cells pooled from 2 independent experiments. **B-D-E-G**, one-way ANOVA, Dunnett's post-hoc test. ns: non significant; *p<0.05; **p<0.01; ****p<0.0001.

of TNFα-SBP-GFP with ERGIC53, a marker of the ERGIC, in any of the conditions tested (Fig. 1B). Taken together, our data show that IpaJ and VirA block the anterograde trafficking at multiple stages, confirming their independent action in blocking host cell secretion.

To investigate the global effects of *S. flexneri* infection on the secretory transport in a polarized cell system, we used the SILAC technology coupled to LC-MS/MS (16). Polarized Caco-2/TC7 cells labeled with "medium" amino acids were uninfected, and cells labeled with "heavy" amino acids were infected with either WT *S. flexneri* or the mutant *virAipaJ*. After 5 hours of infection, the SILAC-labeled secretome-containing supernatants from the apical and basal side were collected and treated for mass spectrometry analysis in order to determine the relative abundance of peptides between infected and uninfected samples (Fig. S1B). Fold change-based GO enrichment analysis showed that apical and basal secretome proteins were more than 4-times enriched in extracellular proteins in comparison to the human

theoretical proteome, hence revealing the good quality of our analysis. We quantified 148 proteins in the apical and 136 in the basal supernatants that were differentially secreted in WT *S. flexneri* infected cells when compared to uninfected cells (UI), from which 125 (84%) and 79 (58%) proteins, respectively, were less secreted (Fig. 1C, Table S1). This secretion impairment was independent of global changes in the proteome of infected cells (Fig. S1C). In addition, tight junctions and cell viability were not affected during the secretome collection (Fig. S1D-F). Among the differentially secreted proteins, 116 (92.8%) of the apical and 64 (81%) of the basal proteins contained predicted cleavable signal peptides indicating targets of the conventional secretory pathway (Fig. 1D). In contrast, analysis of the same proteins from the *virAipaJ*-infected samples revealed only a marginal impairment on the secretion of signal-peptide containing proteins; indeed, the mean fold-change was less striking than for the WT-infected secretomes (Fig. 1D, Table S1). Taken together, these results indicate that *S. flexneri* infection affects the conventional

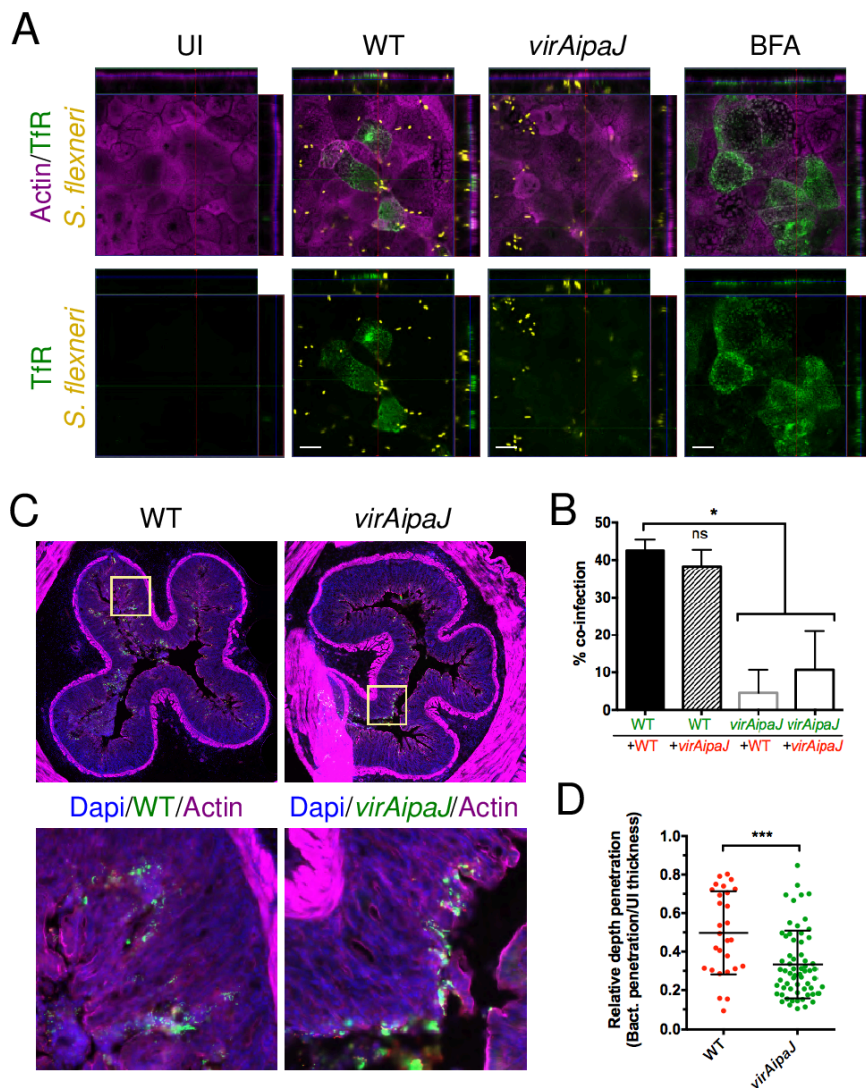


Fig. 4. *S. flexneri* invasion disrupts cell polarity and colonic epithelium(A) *S. flexneri* delocalizes the TfR to the apical domain of polarized Caco-2/TC7 cells. Cells were left uninfected (UI), infected with the WT or *virAipaJ* strains for 5h or treated with BFA for 30 min, prior to fixation without permeabilization and subsequent apical surface staining with an anti-TfR (OKT9) recognizing the extracellular domain of the receptor. Scale bars: 10 μ m. (B) IpaJ and VirA enhance re-infection of polarized cells. Caco-2/TC7 cells were primo-infected with GFP-expressing WT or *virAipaJ* strains (green) for 4 hours, and then re-infected with the same strains expressing dsRed for 2 more hours (red). The % of co-infection was quantified by determining the % of primo-infected cells (GFP positive) that were re-infected with dsRed-expressing bacteria. Mean SD, n = 4. ns: non significant; * p<0.05 (Kruskal-Wallis test followed by Dunn's post-hoc test). (C-D) *S. flexneri* WT has a deeper penetration than *virAipaJ* mutant into the Guinea pig colonic tissue. (C) Colonic tissue from animals infected with GFP-expressing WT or *virAipaJ* mutant, 8 hours post-infection, were stained with Phalloidin-A647 (actin) and Dapi (nuclei). (D) The relative depth penetration of both strains into the colonic tissue was measured by their penetration from the epithelial surface compared to the total epithelial mucosa thickness at 4 hours post-infection. Mean SD. 28<n<48 focus of infection pooled from 2 biological replicates. ***p<0.001 (Mann-Whitney test).

secretory pathway in a global manner, and that this is mediated by the action of both IpaJ and VirA effectors.

Among the proteins less secreted by WT-infected cells, the most represented class were hydrolytic enzymes, like proteases (cathepsin D, carboxypeptidase M) and enzyme regulators. However, we also found cell receptors (LDLR, HGFR), lipid transporters (apolipoproteins), proteins related to cell adhesion and extracellular matrix (ECM) (laminins), and immunomodulators (IL6ST) (Table S1). The secretion inhibition of this wide array of proteins may have severe consequences on cell polarity and intestinal tissue organization and functions.

***S. flexneri* effectors IpaJ and VirA both block the host cell recycling pathway**

As IpaJ and VirA effectors are targeting small GTPases from the Arf and Rab families, which are important for normal endosomal functioning (1, 3), we further investigated if they were also implicated in the previously described reorganization of the endosomal compartment and impairment of transferrin (Tf) receptor (TfR) recycling (9). We loaded Hep2 cells with fluorescent Tf coupled to Alexa Fluor 647 (Tf-AF647), prior to infection with WT, *virA*, *ipaJ* or *virAipaJ* strains (Fig. 2A). In line with what was previously reported (9), after 1 hour of infection with WT *S. flexneri* we observed an extensive formation of membrane tubules labeled with Tf-AF647, which resembled

the phenotype induced by the drug brefeldin A (BFA) (Fig. S2A) (17). A comparable, tubular phenotype was observed when cells were infected with the *virA* mutant strain. In contrast, in cells infected with either the *ipaJ* or *virAipaJ* mutant, Tf-AF647 was located in punctate vesicles throughout the cytoplasm, resembling the uninfected control (Fig. 2A). These findings demonstrate that IpaJ is involved in endosomal compartment tubulation. As shown in the case of BFA-treated cells (17, 18) (Fig. S2B), the formation of endosomal tubules is not necessarily linked to a striking recycling impairment. We therefore assessed TfR recycling kinetics by pulse-chase experiments. Here, cells were loaded with Tf-AF647, uninfected or infected for 1 hour with the GFP-expressing WT or mutant *S. flexneri* strains, and then chased with the unlabeled holo-Tf for different time-points prior to analysis by flow cytometry (FC) (Figs. 2B, S2D). We observed a notable reduction of Tf-AF647 recycling in WT-infected cells, whereby 50% of the internalized Tf-AF647 recycled back to the plasma membrane in 17 minutes, as compared to only 9 minutes for uninfected cells. In addition to the observed time delay induced by the WT strain, Tf recycling was also blocked, as indicated by 29% retention of Tf-AF647 at the 60 minutes kinetic end-point. When cells were infected with the *ipaJ* or *virA* mutant, an intermediate phenotype was observed while the *virAipaJ* double mutant had normal levels of Tf recycling similarly to uninfected conditions (Figs. 2B, S2D).

These results demonstrate that a combined action of these two effectors is required to efficiently block receptor recycling in the host cell. Further, we confirmed that the inhibitory effect of IpaJ and VirA on receptor recycling is due to their catalytic activities. While their ectopic expression in Hep2 cells dramatically decreased the Tf recycling rate (Figs. 2C, S2E), control levels of Tf recycling were obtained when the VirA-R188K/Q280A or IpaJ-C64A mutated versions were expressed (Figs. 2C, S2E). To gain further insights into the mechanisms at play, we overexpressed one of the targets of IpaJ, the small GTPase Arf1 fused to GFP, prior to infection with dsRed-expressing bacterial strains (Figs. 2D, S2F). In uninfected cells the Tf recycling rate remained unchanged despite overexpression of either Arf1-GFP or GFP-VSVG, which served as a transfection control (Figs. 2D, S2C-F). Interestingly, the rate of Tf recycling was faster in cells infected by the IpaJ-expressing strains, WT and *virA*, and overexpressing Arf1-GFP (Figs. 2D, S2F). In contrast, in *ipaJ*-infected cells, the recycling kinetics remained unchanged by Arf1 overexpression. These results strongly suggest that IpaJ slows down Tf recycling by targeting Arf1. Overall, we demonstrate that the two *S. flexneri* effectors, IpaJ and VirA, present catalytic activities that together strongly inhibit two major trafficking pathways, secretion and recycling, that are implicated in the delivery of molecules to the cellular surface.

***S. flexneri* infection affects different host endocytic pathways**

Next, we investigated whether *S. flexneri* directly blocked the endocytic pathways. In the first instance, we aimed to test *S. flexneri* infection on clathrin-dependent endocytosis (CDE). To do this, we performed Tf uptake experiments using Tf, a *bona fide* cargo of CDE (19). Hep2 cells were either left uninfected or were infected for 90 min with GFP-WT *S. flexneri*, prior to incubation with Tf-AF647 at 37°C for different time-points, and followed by FC analysis. In WT-infected cells, we observed a 54% reduction in the endocytosis rate, as well as a significant inhibition of the total Tf uptake at the 30 minutes end-point (Fig. 3A-B), which was independent of the surface expression of TfR (Fig. S3A). This defect on Tf uptake was also observed in WT-infected polarized Caco-2/TC7 cells, after basolateral incubation with fluorescent Tf (Figs. S3C-D). In order to test if other endocytic pathways were affected by *S. flexneri* infection, we assayed for IL-2 receptor (IL-2R) uptake, a well-described marker of a clathrin-independent endocytosis (CIE) pathway (20). Hep2β cells, stably expressing the IL-2Rβ chain, were left uninfected or infected with WT *S. flexneri* strain for 90 min and then incubated with an anti-IL-2Rβ chain antibody coupled to Cy3 for 15 min, fixed and analyzed by fluorescent microscopy (21) (Fig. 3C). We observed a dramatic reduction in IL-2Rβ uptake in WT-infected cells after 15 min of endocytosis when compared to uninfected cells (Fig. 3D). These results indicate that WT *S. flexneri* reduces both clathrin-dependent and -independent endocytosis pathways.

As IpaJ and VirA effectors target key players in regulating intracellular transport, we asked whether they had an impact on this inhibition of endocytosis. Thus, we infected cells with *S. flexneri* WT, *virA*, *ipaJ* and *virAipaJ* strains and performed Tf-AF647 uptake kinetics. We observed a partial recovery of Tf uptake when infecting cells with the three mutant strains (Fig. 3B), indicating that both IpaJ and VirA decrease endocytosis. This IpaJ/VirA-dependent Tf endocytosis inhibition is stronger than BFA, which does not induce significant changes in contrast to uninfected conditions (Fig. 3B), as previously reported (17, 22). In addition, we confirmed that the inhibitory effect of IpaJ and VirA on endocytosis was due to their catalytic activities, as their ectopic expression in Hep2 cells considerably decreased Tf uptake but not when their catalytic-inactive forms were expressed (Fig. 3E). In order to determine whether other effectors were involved in the Tf uptake impairment, we next tested a panel of *S. flexneri* mutants lacking effectors with different cellular targets (Figs. 3B,

S3B). Interestingly, we also found a partial recovery of Tf uptake in cells infected with the *ipaA* mutant, which lacks the vinculin-binding protein IpaA (Fig. 3B) (23). Again, the differences in Tf uptake rate between mutant strains and WT could not be explained by differences of TfR surface expression (Fig. S3A). Overall, these results demonstrate that three *S. flexneri* effectors, IpaJ, VirA and IpaA, inhibit endocytosis in the host cell.

To gain more insight into the mechanisms by which *S. flexneri* affects CDE and CIE, we looked at dynamin 2 (Dnm2), an enzyme implicated in both pathways and involved in the pinching-off of vesicles from the plasma membrane (24). To this end, we left uninfected or infected Hep2β Dnm2-GFP genome-edited cells (25) with WT *S. flexneri* and analyzed the Dnm2-GFP distribution at plasma membrane by total internal reflection fluorescence (TIRF) microscopy (Fig. 3F-G). Upon WT-infection, we observed a 27% reduction of Dnm2-GFP at the plasma membrane (Fig. 3F), which was quantified by image analysis (Fig. 3G). This reduction was not due to a decrease of total Dnm2-GFP levels (Fig. S3E), but likely linked to a reduced recruitment of Dnm2-GFP to the plasma membrane and hence to endocytic sites. Similar results were obtained when we analyzed the clathrin light chain A (CLC) behavior in Hep2β CLC-GFP genome-edited cells (25) (Fig. S3F-G). Interestingly, this phenotype was correlated with IpaJ and VirA expression since cells infected with either the single or the double *virAipaJ* mutants recovered the normal Dnm2-GFP and CLC-GFP recruitment at the plasma membrane (Figs. 3G, S3G). In addition, BFA-treated cells also showed a reduction in Dnm2-GFP at the plasma membrane, although smaller than upon infection with WT bacteria (Fig. 3G). In contrast, IpaA led to a marginal effect on Dnm2-GFP distribution (Fig. 3G). These results indicate that Dnm2, a key host factor involved in both CDE and CIE, is affected by *S. flexneri*, explaining the observed reduction in the uptake of both Tf and IL-2R upon infection. Altogether, our results show how IpaJ and VirA effectors induce multifactorial defects on the general intracellular trafficking of host cells.

IpaJ and VirA disorganize cell polarity and colonic tissue structure

According to our results, IpaJ and VirA are responsible for blocking three intracellular trafficking pathways: secretion, recycling and endocytosis. We therefore asked whether this vesicular trafficking blockage affected the maintenance of cell polarity. Therefore, we infected polarized Caco-2/TC7 cells and stained the surface TfR, which is usually expressed in the basolateral domain of polarized cells. We observed a pool of the TfR localizing at the apical cell domain upon WT *S. flexneri* infection, similarly to what has been previously reported in BFA-treated cells (26) (Fig. 4A). On the contrary, the TfR did not localize at the apical domain of uninfected or *virAipaJ*-infected cells (Fig. 4A). These results indicate that IpaJ and VirA lead to a loss in the polarized transport of TfR, hence highlighting the *S. flexneri*-mediated disorganization of epithelial polarity.

We next asked whether these two effectors, by disrupting cell polarity and epithelial barrier integrity, promoted new invasion events in a second round of bacterial infection (Figs. 4B, S4A). For that, we first infected cells with either GFP-expressing WT or *virAipaJ* strains, and then with the same strains but expressing dsRed. We then quantified the percentage of cells co-infected by the GFP and dsRed strains (Figs. 4B, S4A). We observed that cells primo-infected with the WT strain were more prone to be re-infected with either the WT or the *virAipaJ* strain when comparing with *virAipaJ* primo-infected cells, which were poorly re-infected (Fig. 4B). This result indicates that IpaJ and VirA favor multiple invasion events, thereby enhancing the efficiency of infection.

Next, we used an *in vivo* model of infection to analyze whether the trafficking impairment caused by IpaJ and VirA induced changes in the colonic epithelial structure and function. We in-

fectured Guinea pigs intrarectally (27, 28) with *S. flexneri* WT or the double mutant *virAipaJ*. First, we observed a compact Golgi structure in colonocytes from *virAipaJ*-infected animals as compared to a fragmented Golgi apparatus observed in WT infected animals, confirming the combined action of IpaJ and VirA on disrupting Golgi structure *in vivo* (Fig. S4B). We then analyzed the relative depth penetration of WT and *virAipaJ* strains from the epithelial surface within the colonic tissue (Figs. 4C-D, S4B). We observed and quantified a 40% decrease in the penetration depth of the *virAipaJ* mutant in contrast to the WT strain. This difference cannot be explained by a spreading defect in the *virAipaJ* mutant, as the plaques formed on a cell monolayer by the *virAipaJ* mutant after 48 hours of infection are only 3% smaller than the ones formed by the WT strain (Fig. S4C). Overall, these results indicate that IpaJ and VirA, by the induction of a general trafficking impairment, are critical for intestinal epithelial invasion *in vivo*.

Discussion

In this study, we showed how two *S. flexneri* effectors, IpaJ and VirA, are necessary and sufficient to block several key intracellular trafficking pathways in invaded cells, inducing a “frozen” state in which cells are no longer able to exchange molecules with their environment. These results were observed *in vitro* both in non-polarized and polarized cells. Moreover, we were able to show *in vivo* the impact of some of the functions of these effectors on the efficient intestinal invasion by the bacteria.

Our work confirmed, in the context of cellular *S. flexneri* infection, the secretion blockage described when overexpressing either of the effectors, IpaJ or VirA (10, 13). This is not trivial as EspG for instance, the enterohaemorrhagic and enteropathogenic *Escherichia coli* (EHEC/EPEC) homolog of *Shigella* VirA, does not affect the secretory transport during EHEC infection (29), but only during ectopic overexpression. This suggests that Rab1 is not targeted *in vivo* by EHEC EspG, and illustrates how the overexpression of certain virulence factors might induce phenotypes that are not observed during natural infection. However, the fact that VirA blocks the secretory transport in *S. flexneri*-infected cells strongly suggests that Rab1 is a VirA substrate, but does not exclude the possibility that other Rabs might be targeted by this effector. In line with this, we demonstrated that VirA, in combination with IpaJ, impairs the normal recycling of cell receptors. VirA, in contrast to EPEC/EHEC EspG, was shown *in vitro* to have a broader range of specificity towards Rab GTPases (13). This strongly suggests that endosomal Rabs, such as Rab11, Rab35 or Rab22 (30), are targeted and inactivated by VirA, explaining part of the recycling impairment. Interestingly, it was reported that EspG reduces surface receptor levels and receptor recycling in EHEC infected cells (29) and this is due to the modulation of an Arf6:Rab35 signaling axis (31). Moreover, EspG was shown to interact with Arf GTPases and PAK (13, 32). However, unlike in EHEC infection, a scaffolding role of VirA modulating Rab-Arf signaling has not been described so far for *S. flexneri*. On the other hand, our results show that IpaJ and VirA work in concert to induce an additive defect in receptor recycling. Although IpaJ activity slows down Tf recycling by targeting Arf1, this might also happen via the inactivation of other Arf family members (11, 33). Altogether, our work reveals that in the case of *S. flexneri* infection, both IpaJ and VirA are necessary to induce strong recycling inhibition by acting on Arf GTPases and possibly on Rab GTPases.

The targeting of the endosomal compartments by these two effectors has consequences not only restricted to the surface receptor recycling, but also to an endocytosis blockage. How IpaJ and VirA reduce Tf uptake, as well as dynamin 2 and clathrin recruitment to endocytic sites at the plasma membrane remains a key question. One hypothesis is that the concerted action of

these two effectors on the secretory and recycling pathways will induce downstream alterations on the endocytic route, as the intracellular trafficking routes are intimately interlinked. Indeed, these two *S. flexneri* effectors target two families of proteins that are key regulators of many intracellular trafficking events, possibly explaining the endocytosis impairment as an indirect consequence of their activities on small GTPases. One possibility suggested by our results is that impairment of exocytosis pathways by IpaJ and VirA blocks the recruitment of dynamin 2 to the plasma membrane. Interestingly, this inhibition is also observed upon BFA treatment, which targets only Arf proteins. However, the effect of BFA being less strong than *Shigella* infection might explain why this drug does not significantly decrease Tf endocytosis and further suggests that the combined action of IpaJ and VirA on Arf and Rab proteins is needed to strongly affect endocytosis. Moreover, it was also reported that dynamin 2 is recruited to the budding sites of recycling endosomes, as well as to the TGN (34, 35), possibly explaining the decreased dynamin 2 recruitment upon *S. flexneri* infection. The bacterium might also affect endocytosis by targeting actin, an important factor for dynamin 2 recruitment (36, 37), since it possesses several effectors modulating actin polymerization, such as IpaC, IcsA, and IpaA (38). In agreement with this, our results demonstrated that IpaA, a vinculin-binding protein involved in actin reorganization, partially inhibits endocytosis. Moreover, the plasma membrane tension, which is regulated by actin polymerization, was shown to affect endocytosis dynamics in polarized cells (39). Thus, by targeting actin dynamic regulators, *S. flexneri* might modulate the plasma membrane tension thereby inhibiting the endocytosis rate of the host cell.

Finally, the global secretion inhibition determined by our proteomic approach revealed a list of less secreted proteins that participate in cell polarity establishment and differentiation (40) and their modulation by *S. flexneri* might perturb the integrity of the intestinal barrier. Candidates among such proteins are those regulating cell adhesion, ECM composition and lipid transport. In addition, the impairment in the secretion of immunomodulators might affect the host immune response. Moreover, our *in vitro* data show that IpaJ and VirA subvert the epithelial polarity and promote multiple invasion events, and we have preliminary data suggesting that they might regulate intercellular junctions stability. These results are in total agreement with our *in vivo* data showing that IpaJ and VirA induce a deeper *S. flexneri* penetration into the colonic tissue.

Overall, our work shows how *S. flexneri* IpaJ and VirA effectors coordinate and modulate the host cell intracellular trafficking, leading to the subversion of the infected cells and tissue that will result in more efficient bacterial invasion.

Acknowledgments

We are very grateful to Pierre-Henri Commere (PFC, Cytometry Platform of Institut Pasteur) for technical help with the FACS MoFlo Astrios EQ, Gaëlle Boncompain and Frank Perez for RUSH reagents, Laurie Pinaud and Claude Parsot for sharing reagents and helpful discussion and to Katja Brunner for critical reading of the manuscript. We thank PBI (Imagopole) platform of Institut Pasteur for microscope maintenance and technical help. This project was funded by ERC Advanced Grants 232798 and 339579 to PJS, FRM grant to MLF (SPF20121226366), PTR 22-16 grant to AG, “Région Ile-de-France” and Fondation pour la Recherche Médicale grants to DL. LS is part of the Pasteur Paris University (PPU) International PhD Program and has received funding from the European Union’s Horizon 2020 research and innovation programme under the Marie Skłodowska-Curie grant agreement No 665807. **Author contribution** MLF, NS and PJS conceived and designed research. MLF and VM performed most of the experiments. AG participated on TIRFM experiments and LS on IL-2R endocytosis and colocalization analysis. GN performed *in vivo* experiments with MLF. SDL participated on MS post-analysis. JRR and PS generated *virAipaJ* and *ospC1C2C3* mutant strains, respectively. VMasson carried out the MS experimental work, GA analyzed MS data and DL supervised MS and data analysis. MLF and NS wrote the manuscript with the input of all authors. NS and PJS supervised the project.

1. Donaldson JG, Jackson CL (2011) ARF family G proteins and their regulators: roles in membrane transport, development and disease. *Nat Rev Mol Cell Biol* 12(6):362–75.

2. Barr F a (2013) Review series: Rab GTPases and membrane identity: causal or inconsequential? *J Cell Biol* 202(2):191–9.

3. Hutagalung AH, Novick PJ (2011) Role of Rab GTPases in Membrane Traffic and Cell Physiology. *Physiol Rev* 91(1):119–149.

4. Phalipon A, Sansonetti PJ (2007) Shigella 's ways of manipulating the host intestinal innate and adaptive immune system : a tool box for survival ? (September 2006):119–129.

5. Galán JE, Lara-Tejero M, Marlovits TC, Wagner S (2014) Bacterial Type III Secretion Systems: Specialized Nanomachines for Protein Delivery into Target Cells. *Annu Rev Microbiol* 68(1):415–438.

6. Schroeder GN, Hilbi H (2008) Molecular pathogenesis of Shigella spp.: controlling host cell signaling, invasion, and death by type III secretion. *Clin Microbiol Rev* 21(1):134–56.

7. Ashida H, Mimuro H, Sasaki K (2015) Shigella manipulates host immune responses by delivering effector proteins with specific roles. *Front Immunol* 6(MAY). doi:10.3389/fimmu.2015.00219.

8. Parsot C (2009) Shigella type III secretion effectors: how, where, when, for what purposes? *Curr Opin Microbiol* 12(1):110–6.

9. Mounier J, et al. (2012) Shigella Effector IpaB-Induced Cholesterol Relocation Disrupts the Golgi Complex and Recycling Network to Inhibit Host Cell Secretion. *Cell Host Microbe* 12(3):381–9.

10. Burnaevskiy N, et al. (2013) Proteolytic elimination of N-myristoyl modifications by the Shigella virulence factor IpaJ. *Nature* 1:1–17.

11. Burnaevskiy N, Peng T, Reddick LE, Hang HC, Alto NM (2015) Myristoylome profiling reveals a concerted mechanism of ARF GTPase deacylation by the bacterial protease IpaJ. *Mol Cell* 58(1):110–122.

12. Dobbs N, et al. (2015) STING activation by translocation from the ER is associated with infection and autoinflammatory disease. *Cell Host Microbe* 18(2):157–168.

13. Dong N, et al. (2012) Structurally distinct bacterial TBC-like GAPs link Arf GTPase to Rab1 inactivation to counteract host defenses. *Cell* 150(5):1029–1041.

14. Campbell-Volais FX, Sachse M, Sansonetti PJ, Parsot C (2015) Escape of actively secreting shigella flexneri from ATG8/LC3-Positive vacuoles formed during cell-to-cell spread is facilitated by IcsB and VirA. *MBio* 6(3):1–11.

15. Boncompain G, et al. (2012) Synchronization of secretory protein traffic in populations of cells. *Nat Methods* 9(5):493–8.

16. Ong S-E, et al. (2002) Stable Isotope Labeling by Amino Acids in Cell Culture, SILAC, as a Simple and Accurate Approach to Expression Proteomics. *Mol Cell Proteomics* 1(5):376–386.

17. Lippincott-Schwartz J, et al. (1991) Brefeldin A's effects on endosomes, lysosomes, and the TGN suggest a general mechanism for regulating organelle structure and membrane traffic. *Cell* 67(3):601–16.

18. De Figueiredo P, et al. (2001) Inhibition of Transferrin Recycling and Endosome Tubulation by Phospholipase A2Antagonists. *J Biol Chem* 276(50):47361–47370.

19. Robinson MS (2015) Forty Years of Clathrin-coated Vesicles. *Traffic* 16(12):1210–1238.

20. Lamaze C, et al. (2001) Interleukin 2 receptors and detergent-resistant membrane domains define a clathrin-independent endocytic pathway. *Mol Cell* 7(3):661–671.

21. Basquin C, et al. (2015) Membrane protrusion powers clathrin-independent endocytosis of interleukin-2 receptor. *EMBO J* 34(16):1–15.

22. Hunziker W, Andrew Whitney J, Mellman I (1991) Selective inhibition of transcytosis by brefeldin A in MDCK cells. *Cell* 67(3):617–627.

23. Tran Van Nhieu G, Ben-Ze'ev A, Sansonetti PJ (1997) Modulation of bacterial entry into epithelial cells by association between vinculin and the Shigella IpaA invasin. *EMBO J* 16(10):2717–2729.

24. Antony B, et al. (2016) Membrane fission by dynamin: what we know and what we need to know. *EMBO J*. doi:10.15252/embj.201694613.

25. Bertot L, et al. (2018) Quantitative and Statistical Study of the Dynamics of Clathrin-Dependent and -Independent Endocytosis Reveal a Differential Role of EndophilinA2. *Cell Rep* 22(6):1574–1588.

26. Wang E, Pennington JG, Goldenring JR, Hunziker W, Dunn KW (2001) Brefeldin A rapidly disrupts plasma membrane polarity by blocking polar sorting in common endosomes of MDCK cells.

27. Arena ET, et al. (2015) Bioimage analysis of Shigella infection reveals targeting of colonic crypts. *Proc Natl Acad Sci* 112(25):E3282–E3290.

28. Shim D-H, et al. (2007) New Animal Model of Shigellosis in the Guinea Pig: Its Usefulness for Protective Efficacy Studies. *J Immunol* 178(4):2476–2482.

29. Clements A, Stoneham CA, Furniss RCD, Frankel G (2014) Enterohaemorrhagic Escherichia coli inhibits recycling endosome function and trafficking of surface receptors. *Cell Microbiol* 16(11):1693–1705.

30. Grant BD, Donaldson JG (2009) Pathways and mechanisms of endocytic recycling. *Nat Rev Mol Cell Biol* 10(9):597–608.

31. Furniss RCD, Slater S, Frankel G, Clements A (2016) Enterohaemorrhagic E. coli modulates an ARF6:Rab35 signaling axis to prevent recycling endosome maturation during infection. *J Mol Biol* 428(17):3399–3407.

32. Selyunin AS, et al. (2011) The assembly of a GTPase-kinase signalling complex by a bacterial catalytic scaffold. *Nature* 469(7328):107–11.

33. Volpicelli-Daley LA, Li Y, Zhang C, Kahn RA (2005) Isoform-selective Effects of the

Bacterial strains
Shigella flexneri 5a strain M90T, harboring a streptomycin resistance mutation (41), was used as the WT strain. All the mutants from this study were generated from the WT strain. All the mutant strains used in this study were part of a *S. flexneri* mutant collection (42), except: *ipgD* (43), *virAipal*, *ospE1E2* and *ospC1C2C3*. Tetracycline resistance cassette was removed from *virA* strain to avoid reduction in IcsA protein levels by FLP-FRT recombination using the pCP20 plasmid. Frozen bacterial stocks

Depletion of ADP-Ribosylation Factors 1–5 on Membrane Traffic. 16(October):4495–4508.

34. van Dam EM, Stoorvogel W (2002) Dynamin-dependent Transferrin Receptor Recycling by Endosome-derived Clathrin-coated Vesicles. *Mol Biol Cell* 13(1):169–182.

35. Cao H, et al. (2005) Actin and Arp1-dependent recruitment of a cortactin-dynamin complex to the Golgi regulates post-Golgi transport. *Nat Cell Biol*. doi:10.1038/ncb1246.

36. Taylor MJ, Lampe M, Merrifield CJ (2012) A feedback loop between dynamin and actin recruitment during clathrin-mediated endocytosis. *PLoS Biol*. doi:10.1371/journal.pbio.100-1302.

37. Grassart A, et al. (2014) Actin and dynamin2 dynamics and interplay during clathrin-mediated endocytosis. *J Cell Biol*. doi:10.1083/jcb.201403041.

38. Valencia-Gallardo CM, Carayol N, Tran Van Nhieu G (2015) Cytoskeletal mechanics during Shigella invasion and dissemination in epithelial cells. *Cell Microbiol* 17(2):174–182.

39. Boulant S, Kural C, Zeeh JC, Ubelmann F, Kirchhausen T (2011) Actin dynamics counteract membrane tension during clathrin-mediated endocytosis. *Nat Cell Biol*. doi:10.1038/ncb2307.

40. García-Lorenzo A, Rodríguez-Piñero AM, Rodríguez-Berrocal FJ, de la Cadena MP, Martínez-Zorzano VS (2012) Changes on the Caco-2 secretome through differentiation analyzed by 2-D differential in-gel electrophoresis (DIGE). *Int J Mol Sci* 13(11):14401–14420.

41. Allaoui A, Sansonetti PJ, Parsot C (1992) MxiJ, a lipoprotein involved in secretion of Shigella Ipa invasins, is homologous to YscJ, a secretion factor of the Yersinia Yop proteins. *J Bacteriol* 174(23):7661–7669.

42. Sidik S, et al. (2014) A *Shigella flexneri* Virulence Plasmid Encoded Factor Controls Production of Outer Membrane Vesicles. *G3: Genes|Genomes|Genetics* 4(12):2493–2503.

43. Allaoui A, Menard R, Sansonetti PJ, Parsot C (1993) Characterization of the Shigella flexneri ipgD and ipgF genes, which are located in the proximal part of the mxi locus. *Infect Immun* 61(5):1707–1714.

44. Grassart A, Dujeancourt A, Lazarow PB, Dautry-Varsat A, Sauvonnnet N (2008) Clathrin-independent endocytosis used by the IL-2 receptor is regulated by Rac1, Pak1 and Pak2. *EMBO Rep* 9(4):356–362.

45. Fourriere L, Divoux S, Roceri M, Perez F, Boncompain G (2016) Microtubule-independent secretion requires functional maturation of Golgi elements. *J Cell Sci* 129(17):3238–3250.

46. Labigne-Roussel AF, Lark D, Schoolnik G, Falkow S (1984) Cloning and expression of an afimbrial adhesin (AFA-I) responsible for P blood group-independent, mannose-resistant hemagglutination from a pyelonephritic Escherichia coli strain. *Infect Immun*.

47. Valdivia RH, Falkow S (1996) Bacterial genetics by flow cytometry: Rapid isolation of Salmonella typhimurium acid-inducible promoters by differential fluorescence induction. *Mol Microbiol* 22(2):367–378.

48. Sörensen M, et al. (2003) Rapidly maturing red fluorescent protein variants with strongly enhanced brightness in bacteria. *FEBS Lett* 552(2–3):110–114.

49. Campbell-Volais F-X, et al. (2014) A fluorescent reporter reveals on/off regulation of the Shigella type III secretion apparatus during entry and cell-to-cell spread. *Cell Host Microbe* 15(2):177–89.

50. Poulet P, Carpentier S, Barillot E (2007) myProMS, a web server for management and validation of mass spectrometry-based proteomic data. *Proteomics* 7(15):2553–2556.

51. Valot B, Langella O, Nano E, Zivy M (2011) MassChroQ: A versatile tool for mass spectrometry quantification. *Proteomics* 11(17):3572–3577.

52. Ritchie M, et al. (2015) limma powers differential expression analyses for RNA-sequencing and microarray studies. *Nucleic Acids Res* 43(7):e47.

53. Benjamini Y, Hochberg Y, Benjamini, Y. and Hochberg Y (1995) Controlling the false discovery rate: a practical and powerful approach to multiple testing. *J R Stat Soc Ser B Methodol* 57(1):289–300.

54. Vizcaino JA, et al. (2016) 2016 update of the PRIDE database and its related tools. *Nucleic Acids Res* 44(D1):D447–D456.

55. Kowal J, et al. (2016) Proteomic comparison defines novel markers to characterize heterogeneous populations of extracellular vesicle subtypes. *Proc Natl Acad Sci* 113(8):E968–E977.

56. Petersen TN, Brunak S, Von Heijne G, Nielsen H (2011) SignalP 4.0: Discriminating signal peptides from transmembrane regions. *Nat Methods*. doi:10.1038/nmeth.1701.

57. Bendtsen JD, Jensen LJ, Blom N, Von Heijne G, Brunak S (2004) Feature-based prediction of non-classical and leaderless protein secretion. *Protein Eng Des Sel*. doi:10.1093/protein/gzh0-37.

58. Ashburner M, et al. (2000) Gene ontology: Tool for the unification of biology. *Nat Genet* 25(1):25–29.

59. Thomas PD, et al. (2003) PANTHER: A library of protein families and subfamilies indexed by function. *Genome Res*. doi:10.1101/gr.772403.

60. Schindelin J, et al. (2012) Fiji: An Open-Source Platform for Biological- Image Analysis. *Nat Methods* 9(June 2012):676–682.

61. De Chaumont F, et al. (2012) Icy: An open bioimage informatics platform for extended reproducible research. *Nat Methods*. doi:10.1038/nmeth.2075.

62. Lagache T, et al. (2018) Mapping molecular assemblies with fluorescence microscopy and object-based spatial statistics. *Nat Commun* 9(1):102–108.

Methods

were streaked onto trypticase soy agar (TSA) plates containing 0.1% (w/v) Congo red (CR) and grown at 37 °C overnight. Plates were kept at 4 °C for up to two weeks.

Cell lines

Hep2 cells (HeLa derivative) and its derivatives expressing the β-chain of IL-2R, Hep2β, were grown in DMEM 1 g/L (Gibco™) supplemented with 10% heat-inactivated fetal calf serum (HI-FCS, Eurobio) at 5% CO₂ at 37° C (44), in the presence of 1 mg/mL G418 (Sigma) for Hep2β cells. CRISPR-Cas9 genome edited Hep2β Dnm2-

GFP and Hep2β CLC-GFP cells (25), and the RUSH stable HeLa cell line expressing the ER molecular hook Streptavidin-KDEL and the cargo SBP-EGFP-TNFα (45) were described previously. Hep2 and HeLa cells are non-polarized cell, and were always cultured to 70% confluence prior to infection experiments. Caco-2/TC7 cells (a clone of Caco-2 cells, human colorectal adenocarcinoma origin) were grown in DMEM 1 g/L supplemented with 20% HI-FCS, GlutaMAX™ and non-essential amino acids (Gibco™). For complete polarization and differentiation of Caco-2/TC7 cells, 2x10⁵ cells/cm² cells were seeded into 12-well or 6-well Transwell inserts (pore size 0.4 μm, Corning) and cultured for 18-21 days at 10% CO₂ at 37° C; fresh media was added triweekly, except for plaque assay experiments, where cells were cultured on plastic 6-well plates. Transepithelial electrical resistance (TEER) was measured using a Millicell-ERS Volt-ohm meter (Millipore). Dextran permeability was assessed by adding 70 kDa FITC-Dextran 200 μg/mL (Sigma) in Ringer's buffer to the apical compartment of Transwell inserts (uninfected or infected in Ringer's solution: 155 mM NaCl, 3 mM KCl, 3 mM NaH₂PO₄, 5 mM Hepes 10 mM Glucose, pH 7.0, with 2 mM CaCl₂, 1 mM MgCl₂) after a 15 min preincubation in Ringer's buffer or in calcium-free Ringer's (containing 10 mM glucose). Fluorescence pass-through to the basal compartment medium was measured with an Infinite M200 Pro multimode plate-reader (TECAN). Lactate dehydrogenase (LDH) was quantified with the CytoTox 96® Non-Radioactive Cytotoxicity Assay (Promega).

Plasmids

Bacteria transformed with plasmids coding for the *Escherichia coli* AfaE adhesin (46), or GFP (pFPV 25.1) (47), dsRed (48) or mCherry fluorescent proteins, were used as indicated. pTRIO-mCherry plasmid was generated by inserting mCherry CDS in *XmaI*-*NheI* sites of pTRIO plasmid, which is the basic backbone of the pTSAR plasmids series (49). The CDS of *ipaJ* was cloned through *EcoRI*-*Bam*HI into pSU2.1tt plasmid (49), giving the pSU2.1tt-*ipaJ*-Myc plasmid. The catalytic site variant was generated by PCR-based mutagenesis introducing the C64A mutation into *ipaJ* (plasmid pSU2.1tt-*ipaJ*-C64A-Myc). *ipaJ* and *virAipaJ* mutant strains were complemented with pSU2.1tt-*ipaJ*-Myc or pSU2.1tt-*ipaJ*-C64A-Myc plasmids. pSU2.1tt-*VirA*-Myc or pSU2.1tt-*VirA*-RQ-Myc plasmids (14) were used to complement *virAipaJ* or *virA* strains. For the ectopic expression of GFP-*VirA*, GFP-*ipaJ* and their mutated variants in mammalian cells, the CDS of *ipaJ* and *virA* were cloned through *HindIII*-*KpnI* into pEGFP-C1 plasmid.

Antibodies and reagents

The following primary antibodies were used: rabbit anti-*S. flexneri* 5a M90T LPS 1:300, mouse anti-GM130 1:200 (BD, #610823), rabbit anti-GM130 1:100 (Abcam, ab52649), mouse anti-GFP DyLight 680 1:1000 (Rockland, #600-144-215), mouse anti-ERGIC53 1:100 (Sigma, SAB4200585), rabbit anti-Sec24b 1:100 (D7D65) (Cell Signaling Technology, #12042), sheep anti-TGN46 1:100 (Bio-Rad, AHP500GT), purified mouse mAb OKT9 (anti-TfR) 1:100, goat anti-dynamin-2 1:500 (Santa Cruz, sc-6400), rabbit anti-clathrin LCA (H-55) 1:500 (Santa Cruz, sc-28276), rabbit anti-GFP 1:1000 (Rockland, #600-401-215), rabbit anti-actin 1:5000 (Sigma, A2066), chicken anti-GFP 1:1000 (Abcam, ab13970). All the secondary antibodies were from all from Molecular Probes and used at 1:500 dilution. FITC-Dextran 70 (Sigma, #46945), Dapi 1 μg/mL (Sigma). Phalloidin-AF647 1:100 (A22287, Molecular Probes). Brefeldin A (Sigma, B7651) was used at 1 μg/mL.

Bacterial infections of cultured cells

Hep2 and Hep2β cells were plated the day before the experiment onto 12-mm coverslips at a density of 0.4x10⁵ cells/cm² for immunofluorescence, or on glass bottom dishes (Mattek) for total internal reflection fluorescence (TIRF) microscopy experiments, and at a density of 0.4x10⁵ cells/cm² on 6-well plates for flow cytometry (FC) or western blot experiments. Bacterial cultures were prepared by picking a single colony from each strain from TSA-CR plates and grown in 8 mL of trypticase soy broth (TSB) supplemented with the appropriate antibiotics (ampicillin 100 μg/mL, chloramphenicol 10 μg/mL) in a shaking incubator overnight at 30 °C. Bacteria were sub-cultured in fresh 8 mL TSB at 37° C until OD₆₀₀ 0.8 – 1.0, pelleted, washed in PBS and coated with poly-L-lysine (mol wt 70,000 – 100,000, Sigma) 10 μg/mL in PBS for 10 min, washed twice with PBS and resuspended in the infection medium (DMEM supplemented with 20 mM Hepes) to the adequate multiplicity of infection (MOI). Coated bacteria were added to the cells and allowed to adhere for 15 min at room temperature (RT), and then incubated at 37° C in a CO₂ incubator or in a water bath when short time of infection or short kinetics were performed. For infections of Caco-2/TC7 cells grown in transwell filters, AfaE-expressing strains were cultured as described, pelleted, washed with PBS and resuspended in infection medium to the adequate MOI. Apical and basal chambers were washed twice with warm DMEM-Hepes and bacteria were added to the apical chamber at a MOI = 75, incubated for 15 min at RT and switched to a 37 °C CO₂ incubator. After 30 min, the medium was aspirated and replaced for fresh DMEM-Hepes supplemented with gentamicin 50 μg/mL and incubated for the indicated additional time.

For plaque assays, Caco-2/TC7 cell monolayers were cultured on plastic 6-well plates for 3 weeks, infected at a MOI of 5 for 2 hours, washed and followed by the addition of a 0.5% agarose overlay containing 50 μg/mL gentamicin in culture medium. 48 hours later, cells were fixed with ethanol and stained with Giemsa R solution. Plaque sizes were quantified using Fiji (Image J) software.

RUSH assay to assess anterograde trafficking

RUSH stable HeLa cell line expressing the ER molecular hook Streptavidin-KDEL and the cargo SBP-EGFP-TNFα (45) were uninfected or infected with the indicated *S. flexneri* strain expressing mCherry fluorescent protein. After 15 min at RT and 45 min at 37 °C, the medium was replaced by medium containing 40 μM of biotin (Sigma) to initiate the cargo transport from the ER and incubated at 37 °C for additional 60 min. Cells were washed with ice-cold PBS, fixed in PFA 4%-PBS for 20 min on ice and stained for 1 hour at RT with an anti-GFP DyLight 680 antibody (Rockland) to detect the surface-arrived SBP-EGFP-TNFα. After harvesting, surface

anti-GFP DyLight 680 fluorescence was measured by FC (MoFlo Astrios EQ, Beckman) in the infected population of cells (mCherry positive). Results are the mean expressed as the percentage of total (uninfected or infected) cells expressing the RUSH cargo at their surface. Alternatively, cells grown on coverslips were infected as before and subsequent immunofluorescences were performed as indicated in the figures.

SILAC labeling, infections, sample collection and preparation

Human Caco-2/TC7 cells were cultured for 6 passages in SILAC DMEM flex media deficient for L-arginine and L-lysine (Gibco) with 20% heat inactivated dialyzed FBS (dFBS) (Thermo Fischer), 1 g/L glucose (Sigma), GlutaMAX 1X, non essential amino acids, 10 U/mL penicillin/streptomycin (all from Gibco) supplemented with either 13C6, 15N4 L-Arginine-HCl and 13C6, 15N2 L-Lysine-2HCl (Heavy media) or with 13C6 L-Arginine-HCl and 4,4,5,5-D4 L-Lysine-2HCl (Medium media) (arginine at 84mg/mL and lysine at 146 mg/mL, Thermo Fisher Scientific). The stable isotope labeling was confirmed by LC-MS/MS after protein in-gel separation and digestion of blue bands. Labeled cells were seeded on 6-well Transwell inserts and cultured for 21 days in Heavy or Medium SILAC medium changing the medium 3 times per week.

For secretome collection, 24 hours before infections cells were washed with DMEM for SILAC with 20 mM Hepes and medium was replaced with either Medium or Heavy SILAC media but containing 2% dFBS. Cells were uninfected or infected with AfaE-expressing WT or *virAipaJ* strains. To that end, apical and basal chambers of Transwell inserts were washed 3 times with DMEM for SILAC/Hepes, Medium SILAC medium was added to uninfected cells, and bacteria were added in the apical chamber at a MOI 75 in Heavy SILAC medium without FBS or antibiotics. After 15 min at RT and 30 min at 37° C, cells were washed 3 times with DMEM for SILAC/Hepes, 1.5 mL of FBS-free Medium or Heavy SILAC media with 50 μg/mL gentamicin were added at either apical or basal Transwell chambers, and cells were further incubated at 37° C for 4 ½ hours. Apical and basal secretomes were collected (total volume: 3.6 mL/condition), UI and infected samples mixed in a 1:1 ratio, centrifuged (200 x g, 5 min), filtered with 0.22 μm syringe filters (Minisart, Sartorius Stedim Biotech S.A.) and snap-frozen in liquid N₂. For proteome analysis, cells were lysed in RIPA buffer containing protease inhibition cocktail and samples were mixed at a protein stoichiometry ratio of UI:infected 1:1. Samples were kept at -80° C until use. Before trypsin digestion, uninfected and infected secretomes mixing at a 1:1 ratio was done according to cell number in Transwells from which the secretome was prepared (total volume = 3.6 mL), and then concentrated to 500 μL on Amicon Ultra-15, 10000 molecular weight cutoff centrifugation filter units (Millipore). For the filter-aided sample preparation protocol (FASP), a total of 60 mg of urea and 16 μL of M dithiothreitol were added to 500 μL of concentrated secretome, the solution was mixed on a Nanosep (10 KDa, Pall) device, and was incubated at 57 °C for 15 min. The mixture was spun down and was washed two times with 500 μL of 2 M urea in 0.1 Tris/HCl pH 8.5. A total of 100 μL of 0.05 M iodoacetamide was added and was incubated for 30 min at RT in the dark. Two washes with 25 mM ammonium bicarbonate were performed and the secretome was digested with 5 μg of trypsin / LysC (Promega) for 4 hours at 37 °C. The digested peptides were collected by centrifugation, and the filtrate was dried in a vacuum concentrator at room temperature and was re-dissolved in solvent A (2% acetonitrile, 0.1 % formic acid). Peptides were then subjected to LC/MS analysis. For proteome analysis, mixed proteins lysates were separated on 10% SDS-PAGE (Thermo Fisher Scientific) and were digested in-gel with trypsin / LysC (Promega) as described in standard protocols. Extracted peptides were dried in a vacuum concentrator at room temperature and were re-dissolved in solvent A (2% MeCN, 0.1% HCO₂H) before LC/MS analysis.

LC-MS/MS analysis

For the analysis of cell lysates, peptides were separated by reverse-phase chromatography by using an UltiMate 3000 RSLCnano system coupled to an Orbitrap Fusion mass spectrometer (Q-OT-qIT, Thermo Fisher Scientific). Samples were loaded on a nanoViper C18 μ-precolumn (75μm x 2 cm, Acclaim PepMap, Thermo Scientific) at 5 μL/min of solvent A. After a desalting of 8 min, the precolumn was switched on the C18 column (75μm x 50 cm; 3 μm, 100Å, Acclaim PepMap, Thermo Scientific) equilibrated in solvent A. Bound peptides were eluted using a 168 min four step linear gradient (from 5 to 6% (v/v) in one min, 6 to 9% in 18 min, 9 to 30% in 132 min and 30 to 40% in 9 min) of solvent B (100% MeCN, 0.085% HCO₂H) at 60°C and a 300 nL/min flow rate.

For the analysis of secretome samples, peptides were loaded on a C18 μ-precolumn (Thermo Scientific) at 20 μL/min in solvent A. After a desalting step for 3 min, the precolumn was switched on the C18 column (Thermo Scientific) equilibrated in solvent A and peptide were eluted with a 215 minute two step linear gradient of solvent B (from 5 to 20% (v/v) in 147 min and 20 to 40% in 65 min).

We acquired Survey MS scans at a resolution set to a value of 120,000, with a mass range of m/z 400–1500 and a 4 × 10⁵ ion count target. Tandem MS was performed by isolation at 1.6 Th with the quadrupole, HCD fragmentation with normalized collision energy of 28, and rapid scan MS analysis in the ion trap. The MS² ion count target was set to 1 × 10⁴ and only those precursors with charge state from 2 to 7 were sampled for MS² acquisition. The instrument was run in top speed mode with 3 s cycles.

LC-MS/MS Data Processing and Protein Identification

Data were acquired using the Xcalibur software (v 3.0) and the resulting spectra were interrogated by Sequest HT through Thermo Scientific Proteome Discoverer (v 2.1) with the SwissProt human database (012016). The mass tolerances in MS and MS/MS were set to 10 ppm and 0.6 Da, respectively. We set carbamidomethyl cysteine, oxidation of methionine, N-terminal acetylation, heavy ¹³C₁₅N₂-Lysine (Lys8) and ¹³C₆¹⁵N₄-Arginine (Arg10), medium ²H₄-Lysine (Lys4) and ¹³C₆-Arginine (Arg6) as variable modifications. We set specificity of Trypsin digestion and allowed 2 missed cleavage sites.

The resulting files were further processed by using myProMS (v 3.5) (50). The Sequest HT target and decoy search result were validated at 1% false discovery rate (FDR)

with Perculator. For SILAC-based protein quantification, peptides XICs (Extracted Ion Chromatograms) were retrieved from Thermo Scientific Proteome Discoverer or computed with MassChroQ version 1.2.1 (51). Global MAD normalization or not was applied on the total signal to correct the XICs for each biological replicate. Protein ratios were computed as the geometrical mean of related peptides. To estimate ratio significance, a t-test was performed with the R package limma (52) and the false discovery rate has been controlled thanks to the Benjamini-Hochberg procedure (53) with a threshold set to 0.05.

The mass spectrometry proteomics data have been deposited to the ProteomeX-change Consortium via the PRIDE (54) partner repository with the dataset identifier PXD012291.

Bioinformatics analysis

myProMS (v 3.5) (50) was used to analyze SILAC results. Proteins from infected secretomes were considered as differentially secreted from uninfected secretomes when showing a fold change above or less than 2, $p < 0.05$ and at least 3 detected peptides. Fold change-based gene ontology (GO) enrichment analysis was performed as in (55). SignalP 4.0 (56) was used to determine which proteins contained a signal peptide (predicted or confirmed). SecretomeP 2.0 (57) was used to detect non-conventional secretion; proteins above a cut-off of 0.5 were considered as secreted proteins. GO terms (58) were extracted from PANTHER (59) and UniprotKB.

Transferrin (Tf) recycling and endocytosis

For Tf recycling experiments, Hep2 cells cultured in 6-well plates were incubated at RT with DMEM-Hepes (UI) or the indicated bacterial strains expressing GFP or dsRed proteins at a MOI of 100. After 15 minutes of infection, human Tf coupled to Alexa Fluor 647 (Tf-AF647) (Invitrogen) was added at 0.5 $\mu\text{g/mL}$ in DMEM-Hepes-0.1% BSA at 37 °C. After 30 min of incubation to allow Tf-AF647 endocytosis, surface Tf-AF647 was removed by treating cells with ice-cold sodium acetate 20 mM pH 3.0 for 3 minutes at 4 °C before neutralization with DMEM-HEPES pH 10. Cells were incubated back at 37 °C in DMEM-Hepes-0.1% BSA supplemented with 50 $\mu\text{g/mL}$ of human non-fluorescent holo-transferrin to perform a time course. Cells were scraped gently and transferred into ice-cold PBS for flow cytometry (FC) analysis.

For Tf endocytosis, Hep2 cells were uninfected or infected with GFP-expressing relevant strains as previously described. After 60 min of infection at MOI 10, cells were washed twice with warm DMEM-Hepes and incubated for additional 30 min in the same medium containing 0.1% BSA and gentamicin 50 $\mu\text{g/mL}$ to kill extracellular bacteria. Tf uptake time-course was performed by incubating cells in a water bath at 37 °C with DMEM-Hepes-0.1% BSA in the presence of 0.5 $\mu\text{g/mL}$ Tf-AF647 for different time points, followed by an acid stripping of remaining membrane associated Tf-AF647.

To measure surface TfR levels, UI or infected cells were incubated at 4 °C in the presence of Tf-AF647 for 30 minutes. Cells were acid washed or untreated, and the total surface Tf-AF647 fluorescence was quantified by FC.

Where indicated, cells were transfected with the relevant plasmids the day before the Tf recycling or endocytosis experiments by electroporation (10 μg DNA/4.5x10⁶ cells) or using Lipofectamine 3000 (Thermo Fischer Scientific).

The Geometrical Mean Fluorescence of intracellular Tf-AF647 was measured in gated living cells (using Dapi or Live/Dead Fixable Violet Cell Stain Kit, L34955, Molecular Probes) by FC in a BD FACSCanto II Flow Cytometer (BD Biosciences) or an Attune NxT Flow Cytometer (Thermo Fischer Scientific). Tf recycling results were expressed as the percentage of the remaining intracellular Tf-AF647 at each time point respect to time 0 of recycling. Tf recycling rate was determined from the slope of ln2 data during the first 30 minutes of kinetics. Tf endocytosis results were expressed as Tf endocytosis rate, calculated as the internal Tf-AF647 fluorescence over time, during the first 10 minutes of kinetics.

IL-2R β endocytosis

Hep2 β cells seeded on 12-mm coverslips were uninfected or infected with GFP-expressing bacteria. After 90 min of infection, a time-course of IL-2R β endocytosis was performed by incubating cells with an anti-IL-2R β antibody (mouse Ab 561) conjugated to Cy3 (1:1000) (44) at 37 °C for different time points. Cells were fixed, permeabilized and stained with HCS CellMask Blue Stain (Molecular Probes) and Phalloidin-AF647 or Tf-AF647. Imaging was performed by TIRF microscopy. IL-2R β endocytosis was quantified with ICY software as described in (21).

Animals, infections and sample preparation

Guinea pigs were infected according to previously described protocols (27, 28). Female specific pathogen-free Hartley guinea pigs (120–250 g) were purchased from Charles River Laboratories, maintained in animal care facilities of Institut Pasteur,

and provided with food and water *ad libitum*. Animal experiments were carried out under approval by the "Use Committee of Institut Pasteur and by the French Ministry of Agriculture no. 2013-0113". Briefly, animals were anesthetized intraperitoneally using a mixture of ketamine (100 mg/kg; Merial) and xylazine hydrochloride (10 mg/kg; Bayer) before intrarectal inoculation of *S. flexneri* strains at 5x10¹⁰ cfu per 200 μL . Animals were sacrificed at 4 and 8 hours postchallenge. The distal 10 cm of colon was harvested and fixed overnight in 4% (vol/vol) PFA in PBS, and incubated in PBS-glycine (100 mM) for 30 min to quench the PFA. Tissues were then immersed successively in 15% and 30% (wt/vol) sucrose at 4 °C overnight. Tissues were cut and embedded in Tissue-Tek OCT compound (Sakura) using a flash-freeze protocol and frozen at -80 °C.

Immunofluorescence

Hep2 and Hep2 β cells were fixed in PFA 4% sucrose 4% in PBS for 20 min and quenched with NH₄Cl 50 mM for 10 min. Permeabilization, blocking, incubations and washes were done with PBS BSA 0.1% saponin 0.05%. Polarized Caco-2/TCT cells were washed, fixed and quenched preparing solutions in PBS with Ca²⁺ and Mg²⁺ (Gibco). Permeabilization was done in PBS Ca²⁺ Mg²⁺ gelatin 0.2%, saponin 0.075% for 1 hour at RT, primary antibodies incubated for 90 min at RT or overnight at 4

°C, secondary antibodies 1 hour at RT, together with Dapi 1 $\mu\text{g/mL}$ and Phalloidin coupled to AlexaFluor (Molecular Probes) if indicated.

For tissue sections, immunofluorescence samples were prepared as follows: 10 μm -thick transversal colon sections were permeabilized in PBS 0.5% Triton X-100 for 30 min, blocked in PBS 1% BSA for 30 min at RT and incubated overnight at 4 °C with the indicated primary antibodies, together with Phalloidin AlexaFluor 647 (1:100) diluted in PBS, 0.1% Triton X-100, 1% BSA. Sections were then washed with PBS and stained for 1–2 hours at RT with AlexaFluor 568 goat anti-mouse or anti-rabbit (A11031 and A11036; Molecular Probes), followed by incubation with Dapi (1 $\mu\text{g/mL}$) for 10 min at RT. Samples were washed with PBS before mounting.

ProLong Gold Antifade (Molecular Probes) was used as mounting medium.

Image acquisition

The following equipment was used for image acquisition: a LSM700 inverted laser scanning confocal microscope (Zeiss), with a 40x/1.4 Oil immersion or a 63x/1.4 Oil immersion objective (Zeiss); an Axio Observer.Z1 microscope (Zeiss) equipped with a swept field confocal Opterra system (Bruker) and an Evolve 512 Delta EMCCD camera (Photometrics), using a 63x PlanAPO-CHROMAT oil immersion/1.4 NA objective (Zeiss); a slide scanner Axio Scan.Z1 (Zeiss), using a 40x dry objective; an inverted confocal microscope LSM 780 Elyra PS.1 (Zeiss), using an alpha Plan Apo 100X/1.46 NA oil objective (Zeiss) (TIRF imaging).

Image analysis and quantification

Microscopy images were processed and quantified with Fiji (ImageJ) (60), ICY software (61) (<http://icy.bioimageanalysis.org>) or Zen (Zeiss). Colocalization quantification was performed on confocal images using the Statistical Object Distance Analysis (SODA) plugin in ICY software described in (62). IL-2R β endocytosis was quantified with ICY software using "HK-Means" and "Active Contours" plugins to automatically detect cell boundaries and "Spot Detector" plugin to measure the number of the IL-2R β spots within the detected cells. The total intensity of IL-2R β spots was normalized to the mean value of the uninfected conditions. Quantification of Dnm2 or CLC density at plasma membrane from TIRF images was performed using ICY "Spot detector" plugin to quantify the number of spot per cell area. Quantification of Tf-A647 uptake by Caco-2/TCT cells was performed with Fiji, by quantifying the total fluorescence per cell from 10 slices of 0.8 μm from a z-stack. Tissue images were acquired with 40X objectives and subsequent stitching was performed using Zen software to build the mosaic images. Quantification of bacteria depth penetration into the intestinal mucosa was done from images illustrated in Fig. S4C with Fiji, by measuring the maximum bacterial distance of penetration from the epithelium surface, respect to the total mucosal thickness.

Data presentation and statistical analysis

Prism 6.0 (GraphPad Software, Inc.) was used to perform statistical analysis. Results are represented as mean \pm SD, except otherwise indicated. The following statistical tests were used: Welch's t-test performed as unpaired two-tailed analysis; one-way ANOVA followed by Dunnett's or Tukey's *post-hoc* multiple comparison tests; Mann-Whitney; Kruskal-Wallis followed by Dunn's *post-hoc* test. $P < 0.05$ was considered significant for all analyses.

Fiji and Zen (Zeiss) were used to process microscopy images. Inkscape software (<http://www.inkscape.org/>) was used for assembling figures.